

Amplification of Winter Sea surface temperature response over East China Seas to global warming acceleration and slowdown

Hongjian Tan  | Rongshuo Cai | Xiuhua Yan | Cuihua Li

Third Institute of Oceanography, Ministry of Natural Resources, Xiamen, China

Correspondence

Rongshuo Cai, Third Institute of Oceanography, Ministry of Natural Resources, Xiamen 361005, China.
Email: rscai@163.com

Funding information

National Key R&D Program of China: 2017YFA0604901; Scientific Research Foundation of Third Institute: TIO2017030; National Natural Science Foundation of China: 42005013; Opening Project of Key Laboratory of Marine Environmental Information Technology, SOA

Abstract

The global mean surface temperature does not increase monotonously over the past decades, with accelerated warming from the late 1970s to 1998 and followed by the warming slowdown during 1998–2013 (the so-called warming hiatus). This study assessed and compared the temporal evolutions of sea surface temperature (SST) trends in the East China Seas (ECS, including Bohai, Yellow and East China Sea) and other key ocean regions. The results revealed an amplified response of ECS SST to both global warming acceleration and hiatus. This amplification was manifested as remarkably enhanced winter warming rates in the ECS of over 1.1 and $0.8^{\circ}\text{C}\cdot\text{decade}^{-1}$ for the 1980–1989 and 1990–1999, respectively, and as an obvious cooling trend of nearly $-0.5^{\circ}\text{C}\cdot\text{decade}^{-1}$ during 1998–2013. The enhanced response can be explained well by the combined effects of the Kuroshio Current (KC) and East Asian Winter Monsoon (EAWM). The weakened EAWM during the 1980s, accompanied by lower wind speeds and higher air temperatures, impeded the releases of latent and sensible heat fluxes from the ocean to the atmosphere, resulting in rapid ECS warming. During 1998–2013, the strengthened EAWM led to the enhanced cooling trend in the ECS. In addition, the volume transport of the KC east of Taiwan strengthened (weakened) during the 1990s (2000s), which might also have contributed to the enhanced warming (cooling) in the ECS. Our research suggests their sensitivity makes the ECS potentially vulnerable to the effects of global climate change, which has important implications regarding regional impact assessments.

KEY WORDS

east Asian Winter Monsoon, East China Seas, global warming, Kuroshio Current

1 | INTRODUCTION

The Fifth Assessment Report of the Intergovernmental Panel on Climate Change (IPCC, 2013) demonstrated with very high confidence that the upper ocean has warmed over past decades, with the highest rates of

increase occurring near the surface (i.e., $\sim 0.1^{\circ}\text{C}\cdot\text{decade}^{-1}$ in the upper 75 m during 1971–2010). Despite worldwide warming, the warming rate was not temporally monotonic. For example, the global mean surface temperature rose rapidly from the late 1970s to 1998 (i.e., acceleration period), while after that, no unequivocal warming was

identified during 1998–2013 (or the estimated rate is significantly lower than the preceding warming rate), a phenomenon that has been termed the warming hiatus (Offie, 2013; Trenberth *et al.*, 2014). Despite some controversies (e.g., Karl *et al.*, 2015), the global warming hiatus was generally known as a natural product of interplay between a secular warming trend and a decadal cooling caused by internal climate variability (Medhaug *et al.*, 2017). Some previous studies suggest that the transition to a negative phase of Pacific Decadal Oscillation (PDO) since the late 1990s, has contributed largely to the recent global warming hiatus (Kosaka and Xie, 2013; Dai *et al.*, 2015). Acceleration or deceleration of warming is commonly considered on a global scale, but they are equally important on the regional scale. Specifically, it is of considerable scientific importance to establish how regional seas respond to the global warming acceleration and/or slowdown, because special oceanic areas have their own specific characteristics and significance in long-term air-sea interactions.

The sea areas off the east coast of the mid-latitude Asian continent are potentially highly vulnerable to the effects of anthropogenic and natural climate variability. We focused in this study on the East China Seas (ECS, including the Bohai, Yellow, East China sea, and their adjacent seas), which are coastal, shelf, and marginal sea areas of the northwest Pacific. Numerous studies have documented enhanced warming in the ECS under conditions of global warming (Yeh and Kim, 2010; Cai *et al.*, 2016, 2017). For example, Cai *et al.* (2016) suggested that the winter sea surface temperature (SST) in ECS has increased by nearly 2°C during 1958–2014, with a mean rising rate (trend) of $\sim 0.3^{\circ}\text{C}\cdot\text{decade}^{-1}$, which far exceeds the globally averaged rate of ocean surface warming. Considering the warming hiatus, Liao *et al.* (2015) revealed a significant cooling trend in the low and mid-latitudes coastlines after 1998, including along most of China's coastline. It would seem that the ECS SST has also exhibited a cooling trend over the past decade. However, of greater interest are questions of how and to what extent the changes in ECS SST have been a response to global climate change, particularly to the warming hiatus.

Apart from the remarkable warming, SST in the ECS also exhibits robust interannual and interdecadal variabilities (Cai *et al.*, 2017). Such variations are potentially indicative of large-scale associations with terrestrial, oceanic, and atmospheric forcing. Previous studies have identified several factors responsible for the variability of the ECS SST. These studies have focused mainly on the influences of river discharge (e.g., Kako *et al.*, 2016), of the ocean dynamics processes (Oey *et al.*, 2013), and of the large-scale atmospheric-oceanic disturbances (Yeh

and Kim, 2010; Wu *et al.*, 2014). Among these factors, the East Asian Monsoon and the Kuroshio Current (KC) are considered as the main factors (Zhang *et al.*, 2010; Cai *et al.*, 2017). The East Asian Monsoon dominates the atmospheric circulation over the ECS. Large SST fluctuations can be induced by changes of low-level wind field through surface evaporation, turbulent heat fluxes, and oceanic Ekman advection (Yeh and Kim, 2010; Wu *et al.*, 2014; Chen *et al.*, 2015). On the other hand, the ECS is located near one of the strongest western boundary currents (i.e., the KC), which carries warm tropical water to the mid-latitudes. The vigorous spreading of heat from the KC has been proven to favour decadal warming in the ECS (Oey *et al.*, 2013). The combination of the close connection with the Eurasian continent and exposure to the open ocean could result in local responses in the ECS distinct from other ocean regions. Distinguishing the relative and combined contributions of the atmospheric and oceanic forcing to recent ECS SST change is another motivation for this research.

In this research, based on the multiple SST datasets, we assessed and compared the SST trend in the ECS, and identified an amplified SST response, that is, greater warming (cooling) compared with the global mean during the warming acceleration (hiatus) period. The remainder of this article is organized as follows. Section 2 provides a brief description of the datasets and methods used in the study. Section 3 describes the estimation of the moving linear trend of the ECS SST, and then compares it with other ocean regions and the global mean. The corresponding atmospheric and oceanic physical processes associated with the changes of the ECS SST are investigated in Sections 4 and 5, respectively. Section 6 provides a discussion relating to this study and the final section summarizes the main results.

2 | DATASETS AND METHODS

This study used the Hadley Centre Sea Ice and Sea Surface Temperature (HadISST) $1^{\circ} \times 1^{\circ}$ resolution dataset (Rayner *et al.*, 2003) for the period 1958–2014. This period was selected because of the sparse coverage of in situ observations before the 1950s. Furthermore, to confirm the HadISST results, several other SST datasets were used: (1) the International Comprehensive Ocean-Atmosphere Data Set (ICOADS), which is the most extensive collection of surface marine observational records from ships, buoys, and other platform types; (2) the $\text{:}\backslash$ in situ Observation-Based Estimates (COBE)-SST product that was developed at the Japan Meteorological Agency, which involves some additional and specific observations over the coastal seas offshore of the East

Asian continent; and (3) the monthly NOAA Optimum Interpolation (OI) SST V2 dataset, which exploits AVHRR infrared satellite SST data with large-scale adjustment of satellite biases to the in situ data. In addition, the global monthly land temperature and SST from the HadCRUT4 dataset (Morice *et al.*, 2012) were employed to calculate the global or hemispheric mean surface temperature time series.

Atmospheric variables including surface air temperature, sea level pressure, and wind field were derived from the National Centers for Environmental Prediction/National Center for Atmospheric Research (NCEP/NCAR) reanalysis dataset with a horizontal resolution of $2.5^\circ \times 2.5^\circ$ (Kalnay *et al.* 1996). The three-dimensional potential temperature, and zonal and meridional velocities of ocean currents, obtained from the Simple Ocean Data Assimilation (SODA 2.2.4) system (Carton and Giese, 2008) with $0.5^\circ \times 0.5^\circ$ horizontal resolution and 40 vertical levels, covering the period 1958–2008, were used to analyse the ocean dynamics processes. In addition, monthly ocean evaporation, and turbulent latent and sensible heat fluxes were obtained from the Objectively Analysed air-sea Fluxes (OAFlux) product. We also used the NCEP's Climate Forecast System Reanalysis (CFSR) for atmospheric and oceanic variables and surface fluxes to distinguish the relative contributions of atmospheric forcing and ocean dynamics processes (Saha *et al.*, 2010). The details of the above datasets used in this study are summarized in Table 1. The monthly PDO and

Atlantic Multi-Decadal Oscillation (AMO) indices are from the NOAA Climate Prediction Center (<https://www.esrl.noaa.gov/psd/data/climateindices/>).

The linear trend of a variable (e.g., SST) was examined using linear fitting with the least square algorithm. This method is sensitive to the choice of start and end points and it is inefficient for determining the secular trend of a time series with obvious fluctuations. For example, the time series of global mean surface temperature for the past few decades cover the period of accelerated warming from the late 1970s to the 1990s and the subsequent levelling off after 1998. Therefore, a conventional linear trend approach is inappropriate. Thus, we employed a running linear trend method, which is affected less by the start and end timings of the series. This method has been applied widely in many previous studies (e.g., Dai *et al.*, 2015). Following Dai *et al.* (2015), we selected a 10-year rolling window; however, it is important to note that the results are not sensitive to this criterion. We also tried 13- and 15-year sliding windows, and although the trend value at a specific year might vary depending upon the length of the window used, the periods of positive and negative trend were generally consistent among the different windows. The larger the length of the moving window adopted, the greater the number of data that will be lost. Moreover, the robustness of the moving linear trend was assessed using a Student's *t*-test.

Other statistical analysis methods including correlation, regression analysis, the conventional empirical

TABLE 1 Datasets used in this study

Dataset	Variables	Resolution	Time span (monthly)
HadISST	SST	$1^\circ \times 1^\circ$	1958–2014
ICOADS	SST	$1^\circ \times 1^\circ$	1960–2014
COBE-SST	SST	$1^\circ \times 1^\circ$	1958–2014
OISST	SST	$1^\circ \times 1^\circ$	1981–2014
HadCRUT4	Surface temperature	$5^\circ \times 5^\circ$	1958–2014
NCEP/NCAR reanalysis	Air temperature; zonal and meridional wind speeds sea level pressure	$2.5^\circ \times 2.5^\circ$	1958–2014
SODA	Potential temperature; zonal and meridional current velocities; wind stress	$0.5^\circ \times 0.5^\circ$	1958–2008
OAFlux	Ocean evaporation; latent heat flux; sensible heat flux	$1^\circ \times 1^\circ$	1958–2014
NCEP-CFSR	Potential temperature; horizontal and vertical current velocity; turbulent heat flux; longwave and shortwave radiation flux	$0.5^\circ \times 0.5^\circ$	1979–2009

orthogonal function (EOF), and the multivariate EOF were used in this study. The multivariate EOF analysis, expanding on the basis of conventional EOF (single variable) and considering simultaneous variations of several variables (fields), could extract the dominant pattern among various fields (Wang, 1992). In this study, the multivariate EOF analysis was performed on the wind field, including the zonal and meridional winds. At this time, we only need to double the spatial dimension of the array when importing data ($U; V$). The data is stored separately according to the elements, and after the operation is completed, the order of storage is followed. Two fields are extracted, and both share a time coefficient (principal component). The Lanczos filter with 2-to-7-year band pass filtering was implemented to identify short-term (interannual) variations (Duchon, 1979). In this paper, we focus mainly on the boreal winter (averaging the monthly means of December, January, and February) because the features of change of surface temperature are

particularly strong during winter for both the warming and the hiatus periods (Trenberth *et al.*, 2014). The statistical confidence level is estimated using Student's *t*-test with $N - 2$ degrees of freedom, with N denoting the sample size (e.g., 57 for 1958–2014). However, given the fact that 2-to-7-year band pass filtering may reduce the degrees of freedom, the actual effective degrees of freedom (N_{eff}) used are estimated by $N_{\text{eff}} = r_1/r_2(N - 2)$, where r_1 and r_2 are autocorrelation coefficients of two filtered variables (Trenberth, 1984).

3 | SST TREND IN THE ECS

Figure 1 provides a climatological description of the atmospheric and oceanic environment in the coastal China seas. Large SST variability is observed in the ECS, the magnitude of which is comparable with that in the tropical ocean, especially in boreal winter (Figure 1). The

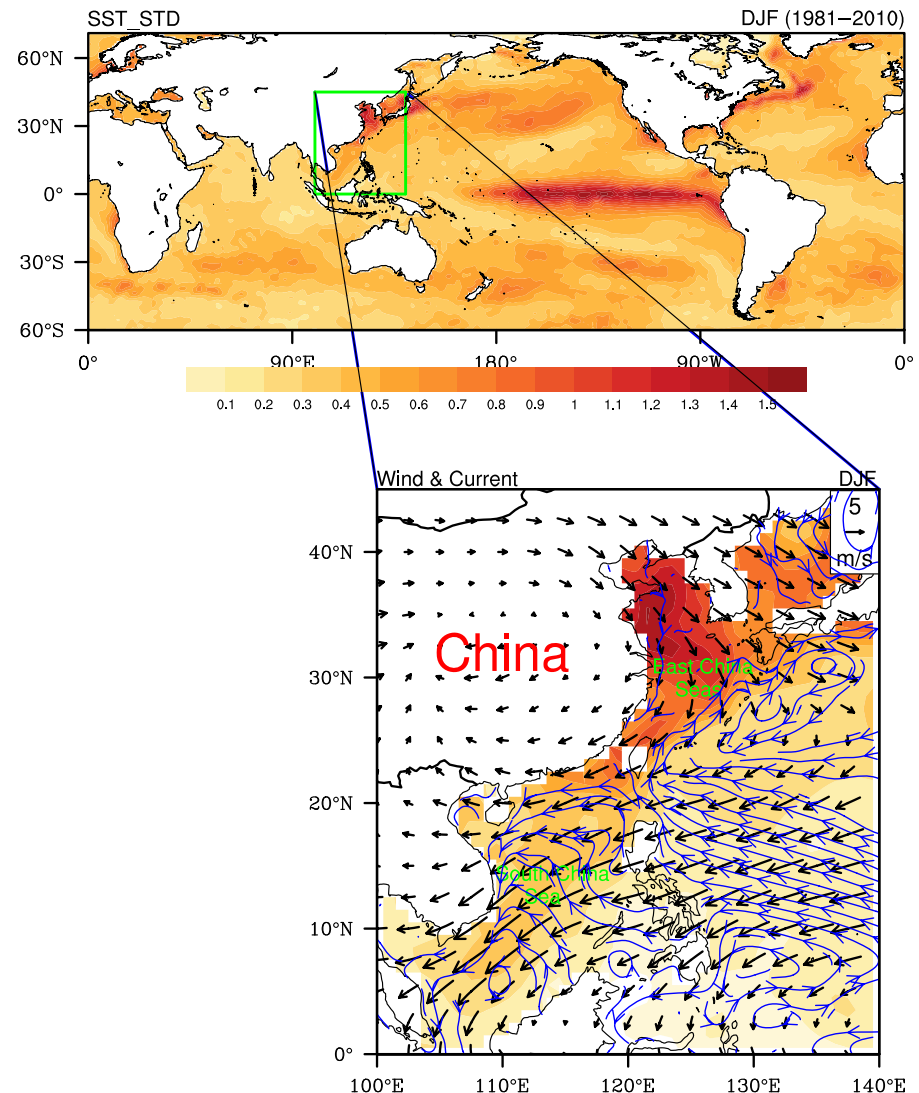


FIGURE 1 Location of the East China Seas and their atmospheric and oceanic conditions; colour shading, vector, and blue streamline denote respectively SST standard deviation ($^{\circ}\text{C}$), climatological wind field ($\text{m}\cdot\text{s}^{-1}$) at 925 hPa, and upper 30 m ocean current ($\text{m}\cdot\text{s}^{-1}$) in winters of 1981–2010. The SST, wind field, and ocean current datasets are from OISST, NCEP/NCAR, and SODA, respectively

change of ECS SST is subject to both the East Asian Monsoon (which is characterized by northwesterlies from the Eurasia continent in winter and a reversed wind field in summer) and KC (a strong warm current that begins off the east coast of the Philippines, and flows northeastward through east of Taiwan to the south of Japan). This unique atmospheric and oceanic configuration may make ECS sensitive to the global climate change.

Previous studies have identified robust surface warming over both land and ocean, with a nearly linear fit to the global mean temperature between the 1970s and 1990s (IPCC, 2013). The biggest outlier in this series is the year 1998 (Watanabe *et al.*, 2014), after which (1998–2013) the warming is less pronounced than before. Consistent with previous studies (e.g., Watanabe *et al.*, 2014; Liao *et al.*, 2015), we refer to the two periods (before and after 1998) as the warming acceleration period and the hiatus period, respectively. Figure 2

depicts the trend of global (the polar ocean is omitted) wintertime SST obtained from four SST datasets during the two periods. During the acceleration period, obvious warming can be found over most of the global oceans, such as the eastern and western tropical Pacific Ocean, tropical Indian Ocean, and coastal waters in mid-latitude Northwestern Atlantic. Noticeably, SST in the mid-latitude of the northwestern Pacific Ocean, especially in the ECS, also experienced a robust upward trend from 1958 to 1998. The results are overall consistent across different datasets (HadISST (Figure 2a), ICOADS (Figure 2c), and COBE-SST (Figure 2e)). In particular, for the OISST (Figure 2g), the observed warming in the ECS is almost the strongest, with a mean rate of SST rise of $>0.08^{\circ}\text{C}\cdot\text{year}^{-1}$ during 1981–1998. The warming rate over the ECS is much faster than that of the global mean SST ($\sim0.1^{\circ}\text{C}\cdot\text{decade}^{-1}$ during 1971–2010), as reported in the Fifth Assessment Report of Intergovernmental Panel on

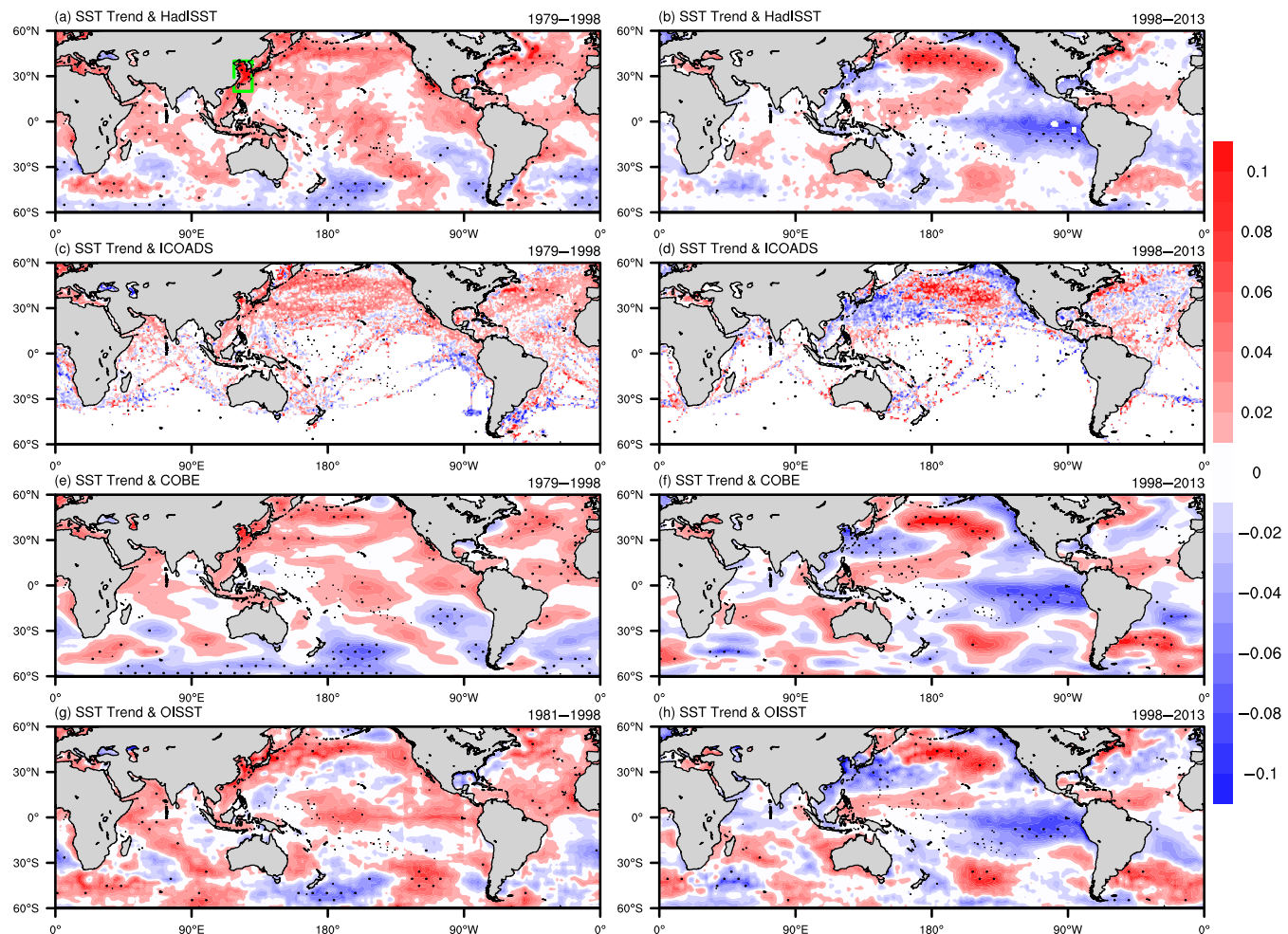


FIGURE 2 Global Sea surface temperature trend in winter during warming acceleration period (before 1998, left column) and hiatus period (1998–2013, right column) based on four datasets; unit: $^{\circ}\text{C}\cdot\text{year}^{-1}$. The four datasets are HadISST (a and b), ICOADS (c and d), COBE-SST (e and f), and OISST (g and h). Dots denote areas above 95% confidence level. The four green boxes in a denote the East China Seas, South China Sea, eastern tropical Pacific, and northwestern Atlantic

Climate Change (IPCC, 2013) and other studies (e.g., Belkin, 2009). Given that the OISST is derived from satellite-based observations with unparalleled spatial resolution and temporal continuity, the OISST results appear most credible. Furthermore, it can be confirmed from other datasets that the ECS represents one of the largest areas of ocean warming during the acceleration period, consistent with previous studies (Yeh and Kim, 2010; Cai *et al.*, 2016).

During the hiatus period (1998–2013), the global trend of SST exhibits considerable regional heterogeneity, with many sea regions reversing their SST trends. Most notably, some of the datasets (HadISST and COBE-SST) show a significantly negative SST trend in the eastern tropical Pacific Ocean (Figure 2b,f). Cooling in the eastern equatorial Pacific, associated with a strengthening of the trade winds, has been identified as the main factor responsible for the global warming hiatus (Kosaka and Xie, 2013; England *et al.*, 2014). Also of note is the reduction of SST trend in the northwestern Pacific Ocean, off the Eurasian continent, with the largest amplitude of cooling in the ECS and adjacent seas. In particular, the trend from the OISST also reveals enhanced cooling in the ECS, the magnitude of which seems comparable with or even stronger than that in the eastern tropical Pacific Ocean (Figure 2h). Although reversals of SST trend are apparent for many oceans, several regions have maintained a continuous increase in SST. For example, during the hiatus period, the high northern latitudes of the Pacific Ocean demonstrate accelerated warming at a rate that appears to exceed that prior to 1998. In addition, the western boundary of the North Atlantic also exhibits a consistent upward trend. Hence, the spatial patterns of SST trend since 1998 are not uniform. The eastern tropical Pacific Ocean and the ECS as well as adjacent seas are amongst those areas with the most pronounced cooling, whereas other regions have continued to experience rising SST (e.g., high latitudes of the North Pacific).

We performed a 10-year moving trend analysis on several SST indices to examine quantitatively and compare the temporal evolution process of the changing rates of the ECS SST and other key oceanic regions. These indices, based on the HadISST, were reconstructed as area-averaged winter SST time series for the ECS ($20\text{--}40^{\circ}\text{N}$, $118\text{--}130^{\circ}\text{E}$), South China Sea ($2\text{--}20^{\circ}\text{N}$, $110\text{--}120^{\circ}\text{E}$), eastern tropical Pacific ($20^{\circ}\text{S}\text{--}20^{\circ}\text{N}$, $90^{\circ}\text{W}\text{--}180^{\circ}\text{W}$), and Gulf Stream ($40\text{--}60^{\circ}\text{N}$, $40\text{--}75^{\circ}\text{W}$). The same analysis was applied to the Northern Hemisphere and global mean surface temperature (land and ocean) indices from HadCRUT4, which were deemed indicators of global mean warming. The period of our analysis was 1958–2014, with a recognition that the results post-1980 could be considered more credible than before. The

moving trend of the ECS SST (Figure 3a) illustrates two periods of accelerated warming (the 1980s and the 1990s) and one period of cooling (the 2000s). The most pronounced warming is seen in the 1980s, with the highest rate of increase of $0.152 \pm 0.017^{\circ}\text{C}\cdot\text{year}^{-1}$ around 1985 (trend between 1981–1990). Although a discrete value may partially depend on the choice of the start and end timings of the time series, the 5-year running mean (thick red lines in Figure 3) also suggested the most pronounced warming around the mid-1980s. Another warming period was in the mid-1990s, despite that the rate of increase is slightly weaker than in the 1980s. The overall trend of SST after 2000 is negative, indicative of cooling in the ECS. The most significant cooling is in the early 2000s with a rate of $-0.053 \pm 0.014^{\circ}\text{C}/\text{year}$. Even after removing the extremely high value of SST in 1998 (due to the 1997/1998 El Niño event), the remainder of the time series retained a general negative trend, suggesting the trend was independent of the choice of timing.

The results are not completely consistent with the moving trend of SST across other oceanic regions. Despite having two similar periods of accelerated warming and one period of cooling, the most obvious warming over the South China Sea can be seen in the mid-1990s (Figure 3b). Furthermore, the magnitudes of the changing rates are lower than that of the ECS for both the warming and cooling periods. Additionally, there is significant interannual variation in the time series of SST over the eastern tropical Pacific. The temporal trend of SST in the eastern tropical Pacific (Figure 3c) appears out of phase with the ECS, that is, the peaks and valleys of the time series of moving trend in the eastern tropical Pacific correspond well with the valleys and peaks of the ECS trend, especially for the 5-year running mean. The correlation coefficient of the two series is -0.48 , above 95% confidence level. Besides, in contrast to the ECS cooling after the late 1990s, the moving trend of SST in the mid-latitude region of the northwestern Atlantic Ocean keeps positive (red line in Figure 3d), indicative of a continuous warming during the hiatus period. The above results, which are based on the HadISST, reveal an enhanced SST response in the ECS to both the acceleration and the hiatus in global warming. The changing rates of the ECS SST (warming and cooling) during both the acceleration and the hiatus periods are larger than that of other sea areas and the global mean (Figure 3e,f). In addition, the three other SST datasets (ICOADS, COBE-SST, and OISST) also presented similar signals and magnitudes of change to the HadISST results in the ECS (Figure 4), confirming the above conjecture.

In summary, it is suggested that the ECS SST varied not only in phase with the global mean, but also featured an enhanced response. The ECS SST showed a faster

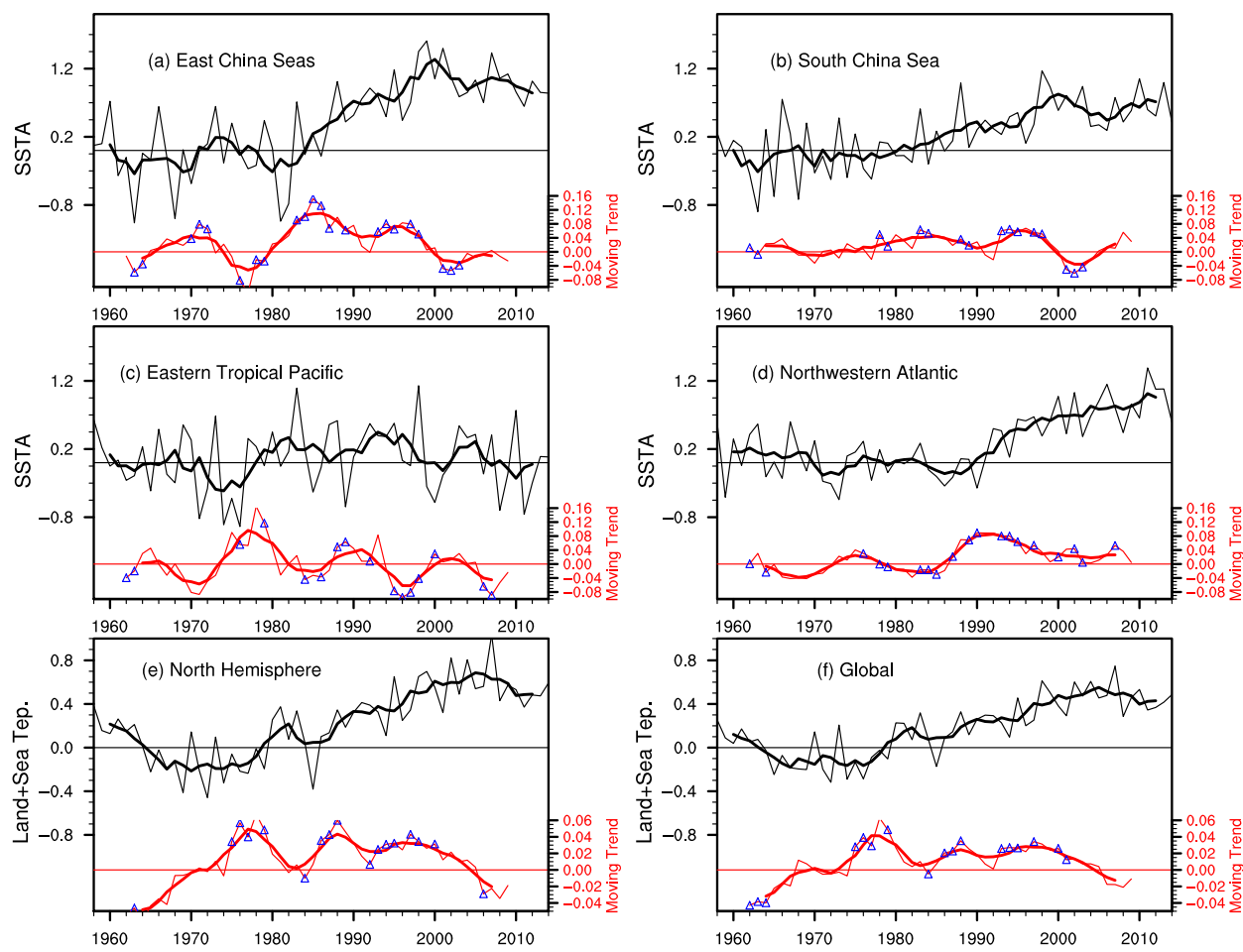


FIGURE 3 Time series of wintertime area-averaged SST anomaly and global mean surface temperature anomaly (black thin line, unit: $^{\circ}\text{C}$) and their 10-year moving trend (red line, unit: $^{\circ}\text{C}\cdot\text{year}^{-1}$) from HadISST. (a)–(f) denote the East China Seas ($20\text{--}40^{\circ}\text{N}$, $118\text{--}130^{\circ}\text{E}$), South China Sea ($2\text{--}21^{\circ}\text{N}$, $110\text{--}120^{\circ}\text{E}$), eastern tropical Pacific ($20^{\circ}\text{S}\text{--}20^{\circ}\text{N}$, $180^{\circ}\text{E}\text{--}90^{\circ}\text{W}$), northwestern Atlantic ($39\text{--}59^{\circ}\text{N}$, $40\text{--}75^{\circ}\text{W}$), Northern Hemisphere mean and global mean. The thick lines (black and red) denote 5-year running mean. Blue triangles denote above 95% confidence level [Colour figure can be viewed at wileyonlinelibrary.com]

trend of increase compared with most other oceanic regions and the global mean during the global accelerated warming periods (1980s and 1990s), whereas it exhibited a significant cooling trend during the hiatus period. In short, the ECS is sensitive and potentially vulnerable to global climate change. Global climate change is generally modulated by large-scale climatic factors such as the PDO and AMO (Dai *et al.*, 2015; Steinman *et al.*, 2015). Actually, the trend of the ECS SST is closely linked to PDO phase switching. The PDO index transformed from its negative phase to a positive phase after the late 1970s, incorporating two positive peaks around the mid-1980s and mid-1990s, before switching back to its negative phase after the late 1990s (Figure 5). It has been suggested that the most recent switch was the major contributor to the warming hiatus (Kosaka and Xie, 2013). The periods with rapid warming (cooling) in the ECS (Figures 3a and 4) are consistent with the

maximum positive (negative) phase of the PDO. It seems plausible that the enhanced SST response over the ECS is simply a regional amplified manifestation of PDO behaviour. The PDO could affect the ECS SST via atmospheric forcing and ocean dynamics processes, such as the East Asian monsoon and the KC, which are investigated in the following sections.

4 | ROLE OF EAST ASIAN WINTER MONSOON IN ENHANCED SST RESPONSE

In winter, the lower atmospheric circulation over the coastal China seas is dominated by the East Asian Winter Monsoon (EAWM), which is characterized by dry and cold northwesterlies originating from the Eurasian continent (Figure 1). The PDO could influence coastal China

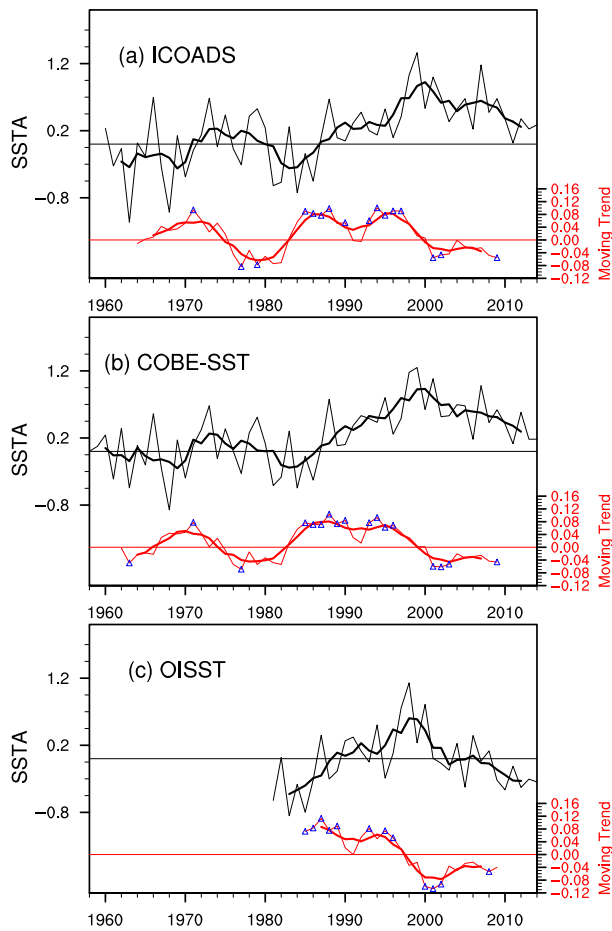


FIGURE 4 Time series of ECS SST anomaly (black thin line, unit: $^{\circ}\text{C}$) and 10-year moving trend (red line, unit: $^{\circ}\text{C} \cdot \text{year}^{-1}$) derived from ICOADS (a), COBE-SST (b), and OISST (c). The thick lines (black and red) denote 5-year running mean. Blue triangles denote significances are above 95% confidence level [Colour figure can be viewed at [wileyonlinelibrary.com](#)]

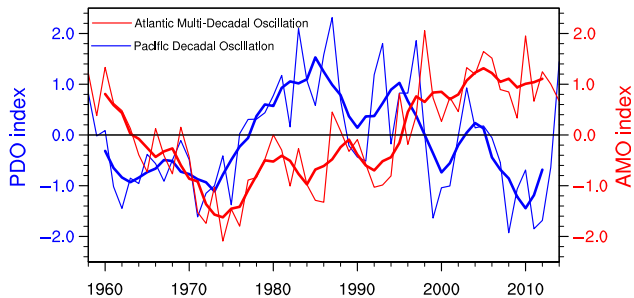


FIGURE 5 Time series of PDO (blue line) and AMO (red line) indices. Thick solid lines denote 5-year running mean [Colour figure can be viewed at [wileyonlinelibrary.com](#)]

seas via a teleconnection that modulates the intensity of EAWM, the specific mechanisms of which have been extensively studied (e.g., Wang *et al.*, 2008; Kim *et al.*, 2014). Due to article length limitations, we sidestep

these issues and focus on the direct influence of the EAWM on the ECS SST.

Figure 6 shows the leading EOF modes of the lower wind field (at 925 hPa) and SST over/in coastal China seas for the winters of 1958–2014. A conventional EOF and a multivariate EOF analysis were performed on the SST and wind field, respectively. Extending on the conventional EOF, which applies to a single variable (e.g., SST), the multivariate EOF analysis covers simultaneous variations of several variables (e.g., zonal and meridional winds), extracting the dominant pattern of the various fields (e.g., EAWM). The first EOF mode (EOF1) of SST accounts for 53.5% of the total variance. It presents a mainly in-phase pattern with the strongest signal in the ECS. The time series of the first principal component (PC1) exhibits an obvious upward trend between the late 1970s and the late 1990s, and a levelling off or even decreasing trend after 1999 (Figure 6b, solid line). Furthermore, the PC1 of SST is closely linked to the PC2 of the lower wind field (Figure 6b, dashed line), with a correlation coefficient of up to -0.72 ($p < .01$). The EOF2 of the lower wind field is characterized by anomalous northwesterlies appearing over Eastern China and ECS, which resembles the climatological pattern of the EAWM. The EAWM weakened after the early 1980s, and it re-amplified after the early 2000s (Wang and Chen, 2014a). It seems that the decadal weakening of the lower wind field over the ECS, which is dominated substantially by the EAWM, could be partially responsible for the rapid warming in the ECS. In addition, the EOF1 of the wind field mainly reflects the robust interannual variation, which is associated with the El Niño Southern Oscillation. However, the high correlation coefficient between SST and the wind field is not limited to the long-term or decadal variations but it also exists in the interannual variations. The repeated EOF analysis after 2-to-7-year band pass filtering also indicated a close linkage (Figure 6d). The correlation coefficient of the PC1s of SST and the wind field is -0.79 ($p < .01$). Therefore, the variations of SST in the ECS are closely linked with the EAWM on both interannual and interdecadal time scales.

The above negative relationships between SST and the wind field (Figure 6b,d) imply atmospheric forcing to the ocean over the ECS, where the dry cold air mass supplied by the EAWM results in considerable heat loss from the sea surface. The turbulent heat flux over the ECS, including latent and sensible heat fluxes, is governed by the EAWM, and it has a positive correlation with the PC1 of the wind field (Figure 7). Moreover, SST in the ECS has a negative relationship with turbulent heat flux (Figure not shown), which is as expected because a robust negative correlation exists between the wind field

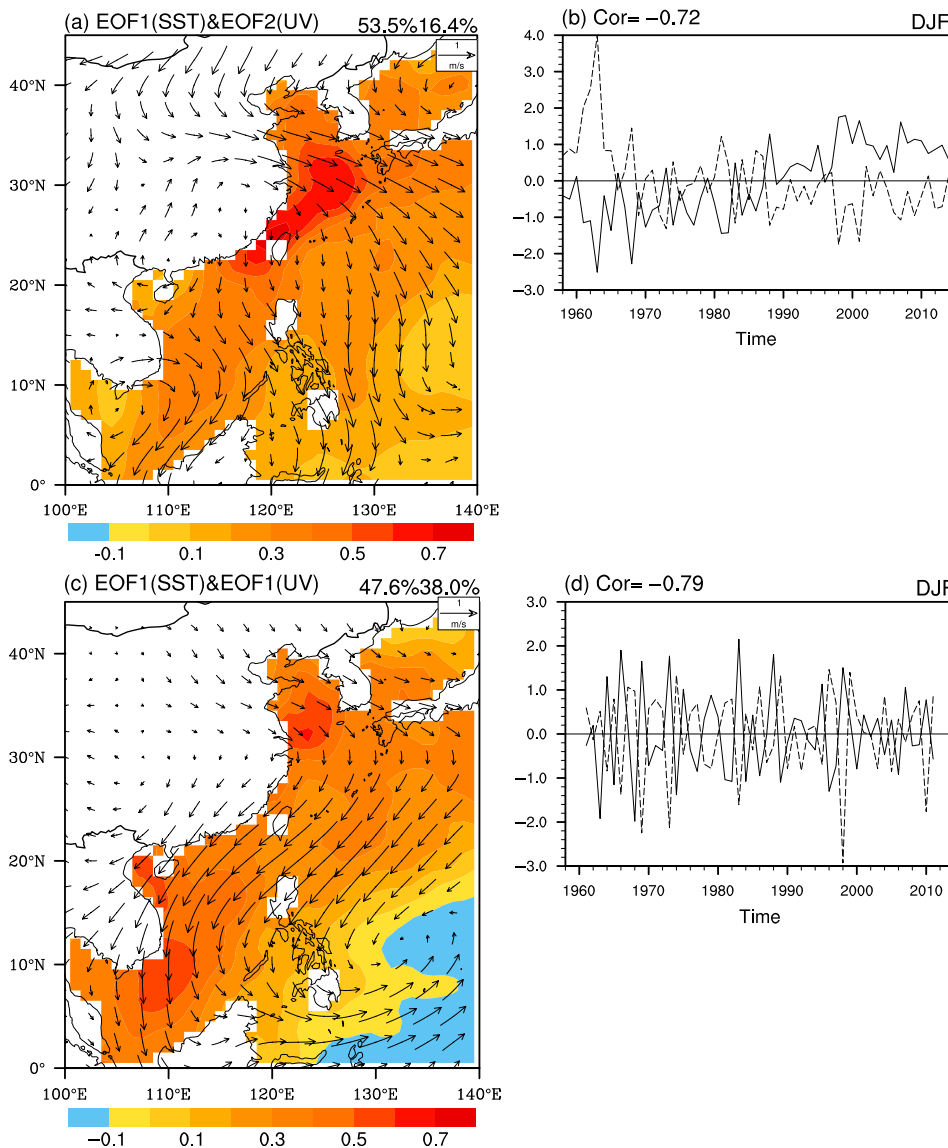


FIGURE 6 The major EOF modes of SST and wind field in winters of 1958–2014. (a) Spatial pattern of EOF1 (EOF2) of SST (925 hPa wind field), (b) time series of corresponding PC1 (solid line) of SST and PC2 (dashed line) of wind field. (c) and (d) are similar to (a) and (b), but for the first modes of SST and wind field after 2-to-7-year band pass filtering. Note that the SST EOF and the wind EOF were calculated separately. The percentage variances explained by the EOF modes are shown above in a and c, from left to right, for SST and wind field, respectively [Colour figure can be viewed at wileyonlinelibrary.com]

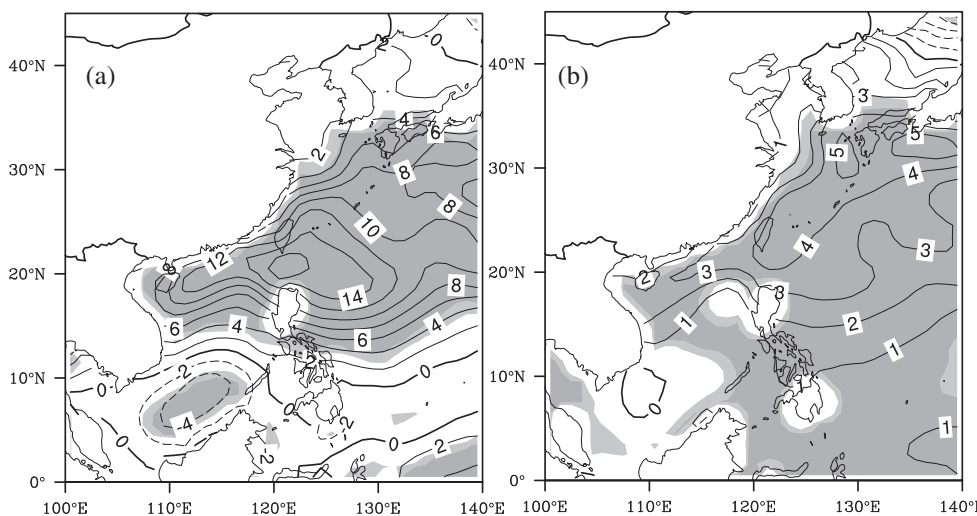


FIGURE 7 Regression of wintertime latent (a) and sensible (b) heat flux on the PC1 of wind field after 2-to-7-year band pass filtering. Unit: $\text{W}\cdot\text{m}^{-2}$. Shading areas denote anomalies that are significant at the 95% confidence level

and SST. Although having a cooling effect on the ECS SST, the decrease (increase) of turbulent heat flux due to a weakened (strengthened) EAWM will result in less (more) heat being released from the ocean, which in turn will lead to relatively warmer (cooler) SST.

To investigate the role of the EAWM in the enhanced response of the ECS SST, an intensity index of the EAWM, proposed by Wang and Chen (2014b), was reconstructed. The definition of this index is:

$$I_{\text{EAWM}} = (2 \times SLP_1 - SLP_2 - SLP_3) / 2 \quad (1)$$

where SLP_1 , SLP_2 , and SLP_3 indicate the normalized area-averaged winter mean sea level pressure (SLP) over Siberia ($40\text{--}60^\circ\text{N}$, $70\text{--}120^\circ\text{E}$), the North Pacific ($30\text{--}50^\circ\text{N}$, $140^\circ\text{E}\text{--}170^\circ\text{W}$), and the Maritime Continent ($20^\circ\text{S}\text{--}10^\circ\text{N}$, $110\text{--}160^\circ\text{E}$), respectively.

Figure 8 illustrates the normalized EAWM index and its 10-year moving trend. A positive index denotes a strong EAWM, featuring a cold winter with lower surface air temperatures and larger wind speeds over East Asia and the adjacent seas, and vice versa. The EAWM appears strong during the late 1970s and early 1980s, and it then decreases dramatically around the mid-1980s (Figure 8). The 10-year moving trend shows the biggest rate of decline in the mid-1980s, which agrees reasonably well with the greatest rate of warming in the ECS. In addition, the EAWM recovers from the weak epoch and it re-amplifies after the early 2000s, which is consistent with the enhanced cooling over the ECS associated with the warming hiatus.

According to the aerodynamic bulk formulae, turbulent latent (sensible) heat fluxes are determined by in situ wind speed and humidity (temperature) differences at the air-sea interface (Tanimoto *et al.*, 2003). Figure 9a shows that the wind speed over the ECS declines sharply in the mid-1980s, as does the latent heat flux released

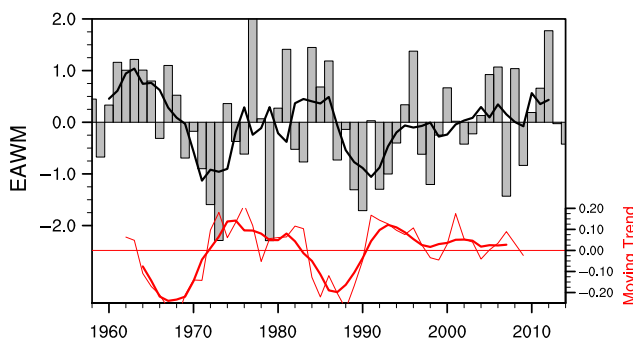


FIGURE 8 The normalized EAWM index (black bar) and its 10-year moving trend (red line). The thick lines (black and red) denote 5-year running mean [Colour figure can be viewed at wileyonlinelibrary.com]

from the ocean (Figure 9e). The increased air specific humidity (Figure 9c) with the maximum rising rate around the mid-1980s cuts back the humidity differences at the air-sea interface, also contributing to a decrease of the latent heat flux. Moreover, the increase in air temperature (Figure 9b) reduced the air-sea temperature difference (Figure 9d), which lessened the release of sensible heat flux (Figure 9f). The decreases in both latent and sensible heat fluxes due to the weakened EAWM contributed to the rapid warming over the ECS in the mid-1980s. After the late 1990s, when the EAWM began to intensify, the higher wind speeds and lower air temperatures increased the latent and sensible heat fluxes released from the upper ocean to the atmosphere, which resulted in the enhanced cooling trend in the ECS. Hence, decadal weakening (strengthening) of the EAWM warmed (cooled) the ECS by modifying the turbulent heat flux. It is noted that the EAWM could partially account for the enhanced warming (cooling) in the ECS during the mid-1980s (after the late 1990s); however, the reason for the warming of the mid-1990s remains unclear, implying the involvement of other physical processes (e.g., ocean dynamic processes), which are discussed below.

5 | ROLE OF KUROSHIO CURRENT IN ENHANCED SST RESPONSE

The ECS and adjacent seas are near the path of the KC, which advects considerable amounts of heat into these regions. The meridional transport (including heat and volume) of the KC has been proven to contribute largely to the anomalous SST in coastal China seas (Guo *et al.*, 2006). Wu *et al.* (2012) suggested that the accelerated warming in mid-latitude western boundary regions over the past century is associated with the intensified heat transport of subtropical western boundary currents. The warm water of the KC intrudes across the ECS shelf at the northeast of Taiwan. Therefore, the KC east of Taiwan is generally identified as an important regulator of the rate of ECS warming (Guo *et al.*, 2006). According to previous research (e.g., Hsin *et al.*, 2008), we focus in the following on the volume transport of the KC to the east of Taiwan at 23°N , where the horizontal width of the high-velocity core (maximum current speed $>0.6 \text{ m}\cdot\text{s}^{-1}$) ranges from 30 to 120 km.

Figure 10 shows the trend of the poleward velocity profile at 23°N to the east of Taiwan. Intensified volume transport of the KC can be observed for the period 1958–2008, based on the SODA dataset. The intensification is particularly significant in the upper 100 m from 121.5 to 122.5°E , where the mean velocity is $>0.4 \text{ m}\cdot\text{s}^{-1}$

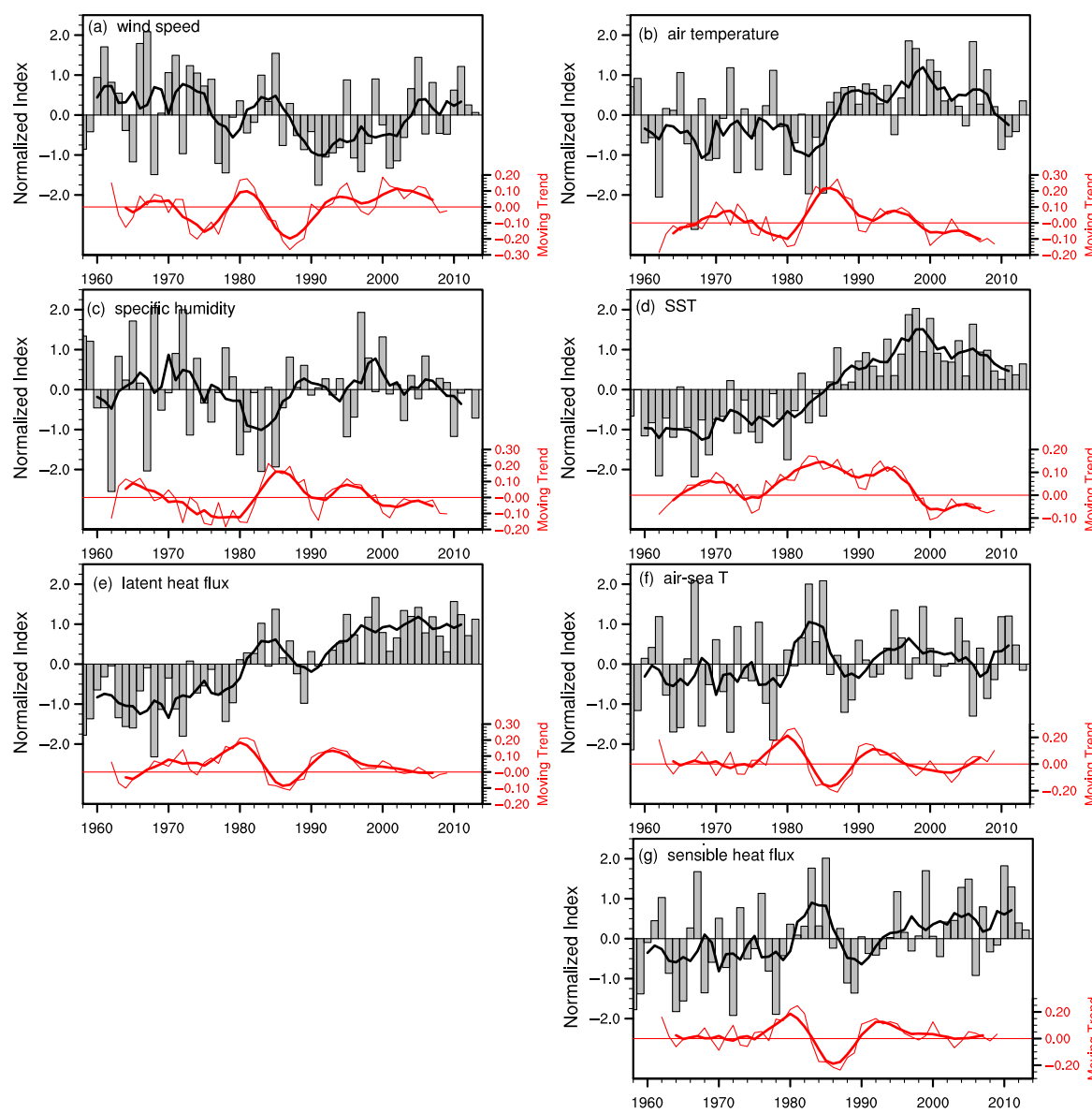


FIGURE 9 Time series (black bar) of area-averaged ($20\text{--}40^{\circ}\text{N}$, $118\text{--}130^{\circ}\text{E}$) indices for wind speed (a), air temperature (b), specific humidity (c), SST (d), latent heat flux (e), air-sea temperature difference (f), and sensible heat flux (g) over the ECS. The indices are normalized for visualization. Red line denotes the corresponding 10-year moving trend. The thick lines (black and red) denote 5-year running mean [Colour figure can be viewed at wileyonlinelibrary.com]

(Figure 10a). For further assessment of the temporal evolution of the KC, an index was constructed as a proxy of KC volume based on the vertically integrated meridional current speed in the upper 100 m at 23°N , $121.5\text{--}122.5^{\circ}\text{E}$ (Figure 10b). The 10-year moving trend reveals a positive peak and negative rates around the mid-1990s and 2000, respectively, suggesting that the KC strengthened and weakened during the above periods (Figure 10b, red line). The maximum rate of rise of the KC volume transport in 1995 corresponds well with the ECS warming around the mid-1990s, which could not be explained by the EAWM. In addition, the weakening of the KC after

the late 1990s is concurrent with the obvious cooling seen in the ECS.

The strengthening (weakening) of the KC was partly responsible for the enhanced warming (cooling) in the ECS during the mid-1990s (after the late 1990s). Variation of the KC could affect the SST in the ECS via the upper-ocean circulation (Figure 11). The intensified volume transport of the KC encourages greater intrusion of warm water across the ECS shelf, leading to a positive SST anomaly in the ECS. Furthermore, the decadal variation of the KC is affected by the modulation of the PDO via the large-scale wind stress curl (Andres *et al.*, 2009).

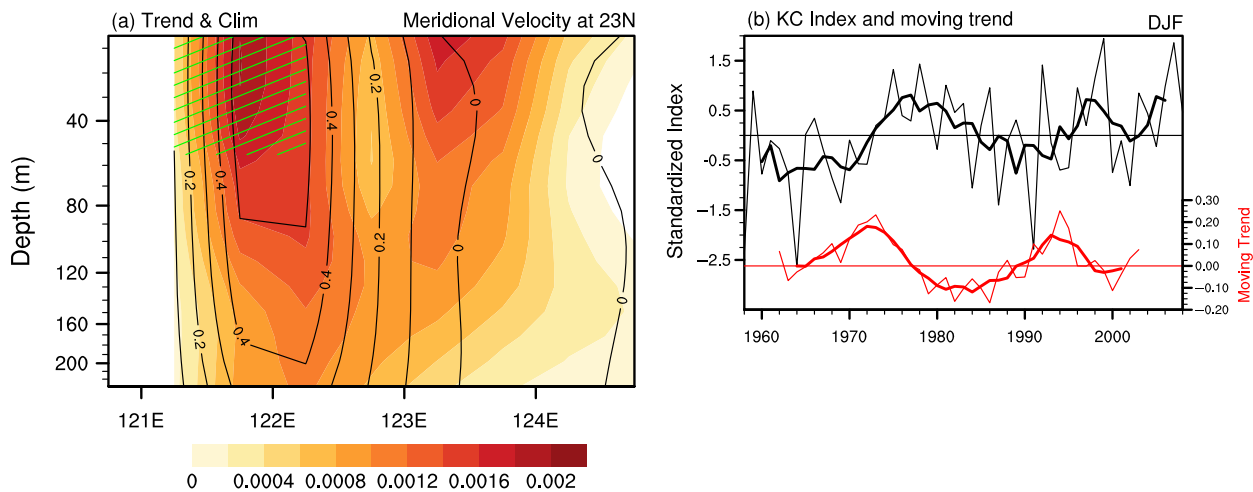


FIGURE 10 Trend of meridional velocity of KC at 23°N from SODA (1958–2008). (a) Depth-longitudinal profile of mean ($\text{m} \cdot \text{s}^{-1}$, contours) and trend ($\text{m} \cdot \text{s}^{-1} \cdot \text{year}^{-1}$, colour shading). (b) Meridional transport index averaged from (23°N, 121.25–122.25°E) upper 50 m (green hatched areas in a) and its 10-year moving trend ($\text{m} \cdot \text{s}^{-1} \cdot \text{year}^{-1}$, red line). The thick lines (black and red) denote 5-year running mean [Colour figure can be viewed at wileyonlinelibrary.com]

The periods of enhancement and weakening of the KC correspond to positive and negative phases of the PDO during the 1990s and 2000s, respectively. However, it remains unclear why the KC weakened in the 1980s (Figure 10b), a period during which the PDO was in its positive phase (Figure 5). It is suggested that the understanding of the mechanisms of PDO influence on the KC remains incomplete because of the complexity of the climatic system and inherent uncertainties in the datasets.

6 | DISCUSSION

The present research revealed an amplified SST response over the ECS to the global warming acceleration and warming hiatus, which was attributed to the combined effects of the EAWM and KC. This study focused on the winter temporal evolution of ECS warming, because the most remarkable ECS warming and global warming hiatus have been reported in winter (Trenberth *et al.*, 2014; Cai *et al.*, 2016). It should be noted that the enhanced SST response was not confined to winter but it also occurred in other seasons (Figure 12). The variation of SST is more obvious in the cold season (winter and spring) than the warm season (summer and autumn), and the physical mechanisms of the summer variation of SST are particularly complex. Apart from the monsoon and the KC, other factors might also be important, such as the variation in the discharge of the Yangtze River related to the large amounts of rainfall over its catchment (Kako *et al.*, 2016) and the intense insolation associated with the subtropical high (Cai *et al.*, 2017). The physical

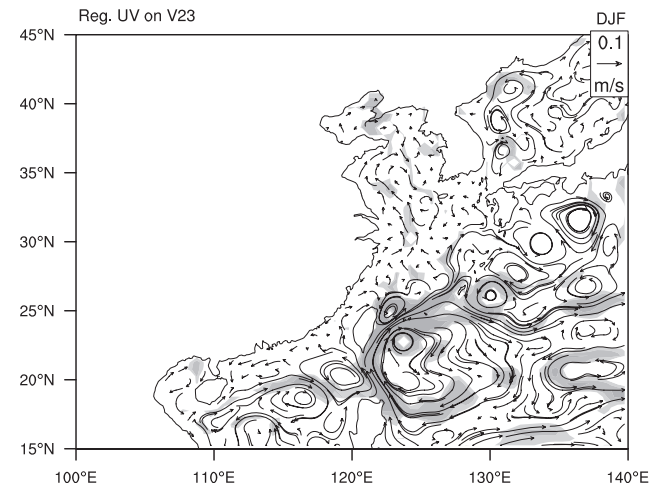


FIGURE 11 Regression of wintertime ocean circulation upper 30 m onto the meridional transport index of KC at 23°N. Shading areas denote anomalies that are significant at the 95% confidence level

mechanisms of the enhanced ECS SST response in summer will be investigated in future work.

Regarding the recent global warming hiatus, Liao *et al.* (2015) investigated coastline-based SST change, and they reported a significant cooling trend along 31.4% of the global coastlines after 1998, including most of China's coastline. The results of our study are similar to their findings; however, we conducted a quantitative comparison and investigated the links between EAWM and KC. In addition, Huang *et al.* (2017) demonstrated that the warming hiatus was more significant over the continental Northern Hemisphere, especially over the mid- to

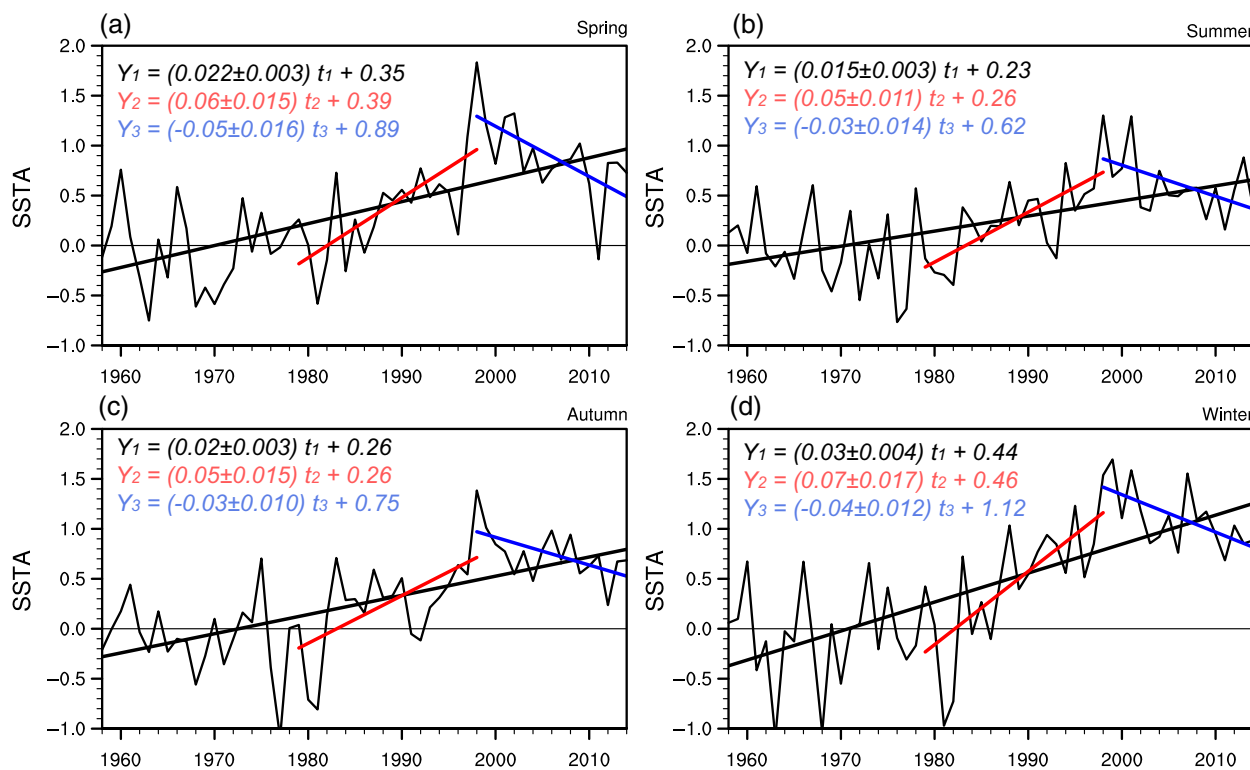


FIGURE 12 SST indices in the ECS and their linear trends in spring (a), summer (b), autumn (c), and winter (d) during different period. The black, red, and blue lines denote linear fitting for 1958–2014, 1979–1998, and 1999–2014, respectively. The corresponding fitting formulas are shown with different colours. Units: °C [Colour figure can be viewed at wileyonlinelibrary.com]

high latitudes of the Eurasian continent. Although it is inadvisable to compare rates of change over land and the ocean because of the different specific heat capacities, the enhanced cooling in the ECS after the late 1990s might in part be associated with the significant cooling trend over the Eurasian continent via the EAWM. Among the several oceanic regions considered in this study, the cooling trend exhibited by the ECS was among the most remarkable (Figures 2 and 3), the extent of which was comparable with the tropical eastern Pacific Ocean, which has been identified as the major driver of the recent warming hiatus.

In addition, the enhanced response of the ECS SST to global warming was associated with PDO. The periods with rapid warming (cooling) in the ECS are in agreement with the maximum positive (negative) phase of the PDO (Figures 3 and 5). Previous studies have indicated that PDO could modulate the decadal variations of both EAWM and KC (Wang *et al.*, 2008; Andres *et al.*, 2009; Kim *et al.*, 2014). On the one hand, changes in SST over North Pacific substantially influence atmospheric teleconnection in the Northern Hemisphere, such as the Eurasian-like pattern and Pacific–North American pattern (Zhou *et al.*, 2014; Jia *et al.*, 2016), and then result in changes in the strength and path of the EAWM (Wang

and Lu, 2017). The phase shift of PDO could also affect the linkage of ENSO and EAWM through modulating ENSO-induced large-scale circulation background, such as the Aleutian low (e.g., Wang *et al.*, 2008). For example, during the positive phase of PDO, the Aleutian low is strong, and could dominate the atmospheric variability over the North Pacific (see Figure S1), which may weaken the ENSO-EAWM relationship. On the other hand, as the Kuroshio is primarily wind-driven, its heat and volume transport is dominated by the basin-scale wind stress curl over the North Pacific, which is also associated with PDO (Andres *et al.*, 2009). The specific mechanisms of PDO affecting the EAWM and KC have been extensively studied (e.g., Wang *et al.*, 2008; Andres *et al.*, 2009; Chen *et al.*, 2013; Kim *et al.*, 2014), and here we sidestep these issues and focus on the direct influences of local atmospheric forcing and ocean dynamics processes on the enhanced ECS SST response.

Of considerable interest and concern is the relative contribution of EAWM and KC to the enhanced SST response in the ECS. To this end, the direct influences of net surface heat flux (linked to EAWM) and oceanic dynamic processes (associated with KC) on local sea temperature in the ECS were diagnosed in terms of sea temperature budget equation. Note that Equation (2) is just a

simplified version of the primitive equation, and one can refer to Moisan and Niiler (1998) for the formal derivation.

$$\frac{\partial T}{\partial t} = -\vec{v} \cdot \nabla T + \frac{1}{\rho c_p h} Q_{\text{net}} + R \quad (2)$$

where T is the anomaly of seawater temperature vertically averaged in the upper mixed layer, and \vec{v} is three-dimensional ocean current velocity (u ; v ; w). ∇ is the gradient operator ($\nabla \equiv \partial/\partial x, \partial/\partial y, \partial/\partial z$). ρ is the mean density of seawater, and c_p is the specific heat of seawater. The mixed layer depth (h) is defined as the depth at which the temperature is 0.5°C below the near-surface value. This criterion presents an optimal estimate of MLD at the mid-latitude (e.g., Kelly and Qiu, 1995). Changes of T' are affected by the total ocean advection, net surface heat flux (Q_{net}), and residual terms (R). Here, R may comprise diffusive heat flux, entrainment, and so on.

Previous studies suggest R is much less than the other two terms, and hence will not be estimated here. The total ocean advection consists of zonal advection, meridional advection, and vertical advection. Each component comprises three subcomponents: the anomalous temperature gradient multiplied by the mean current, mean temperature gradient multiplied by the anomalous current, and anomalous temperature gradient multiplied by the anomalous current. For example, the meridional advection can be decomposed as follows:

$$-\vec{v} \frac{\partial T}{\partial y} = -\bar{v} \frac{\partial T'}{\partial y} - v' \frac{\partial \bar{T}}{\partial y} - v' \frac{\partial T'}{\partial y} \quad (3)$$

where the overbars and primes indicate the monthly climatological mean and anomaly, respectively. In addition, Q_{net} is the sum of the latent heat net flux (Q_{LH}), sensible heat net flux (Q_{SH}), net shortwave radiation flux (Q_{SW}), and net longwave radiation flux (Q_{LW}):

$$Q_{\text{net}} = Q_{\text{LH}} + Q_{\text{SH}} + Q_{\text{SW}} + Q_{\text{LW}} \quad (4)$$

A positive value of Q_{net} is indicative of anomalous heat flux from the ocean to the atmosphere. Because vertical velocity is unavailable in the SODA dataset, we used the CFSR reanalysis instead, which contains all the necessary atmospheric and oceanic variables. The mean turbulent heat fluxes and upper-ocean currents in coastal China seas, derived from the CFSR reanalysis, were compared with corresponding variables from the OAFlux and SODA datasets and the results found generally consistent (Figure not shown). In particular, the moving trend of meridional current velocity derived from the CFSR

reanalysis (1979–2009) at 23°N to the east of Taiwan was similar to that obtained from the SODA dataset (see Figure S2).

We diagnosed the wintertime relationships between the tendency of T (left-hand side of Equation 2) and the oceanic dynamic processes based on the CFSR reanalysis. Of the three advection terms, meridional advection showed the closest link to the tendency of T (Figure 13). In particular, a significant positive correlation was found between the local tendency of T ($\partial T/\partial t$) and the anomalous meridional advection induced by the mean temperature and anomalous meridional current ($-\vec{v}' \partial \bar{T}/\partial y$). The strongest signals were found in the ECS and the KC to the east of Taiwan (Figure 13a). The other two terms ($-\bar{v}' \partial T'/\partial y$ and $-v' \partial \bar{T}'/\partial y$) were found to have little connection with the tendency of T (Figure 13b,c). The total anomalous meridional advection was dominated by the anomalous meridional current (Figure 13d), confirming the large contribution of the KC to the local variation of T in the ECS. In addition, the links between the tendency of T and the anomalous zonal advection and vertical advection were not significant (see Figures S3 and S4).

The following discussion is based on calculations of the relative contributions of the total oceanic advection and Q_{net} during the winters of the 1980s (1981–1990), 1990s (1990–1999), and early 2000s (1999–2005), three periods during which the ECS SST experienced remarkable warming or cooling (Figure 4). During the 1980s, the sea temperature in the upper-mixed layer of the ECS increased by about 1.1°C , while the contributions of Q_{net} and total oceanic advection were 0.8 and 0.2°C , respectively (Figure 14). It appears that most of the warming in the 1980s in the ECS was caused by Q_{net} . In fact, Q_{net} in the ECS was always positive in winter, implying that it has a damping role on changes of SST in the ECS. However, Q_{net} declined from the early 1980s, similar to the variations of latent and sensible heat fluxes (Figure 9c,d); therefore, the positive contribution to local warming in the ECS was mainly due to the reduction in Q_{net} from the ocean to the atmosphere.

During the 1990s, relatively more Q_{net} was released from the ocean, presumably due to increased latent and sensible heat fluxes (Figure 9c,d), which impeded the warming in the ECS. Although Q_{net} played a negative role (-0.5°C) in the ECS warming, sea temperature in the ECS increased by nearly 0.75°C (Figure 14), which might have resulted from the contribution of oceanic advection (0.8°C). The earlier analysis (Figure 10b) indicated that the volume transport of the KC to the east of Taiwan strengthened remarkably in the mid-1990s. Hence, the enhanced warming in the ECS during the 1990s could be attributed largely to oceanic advection associated with the increased meridional transport of the

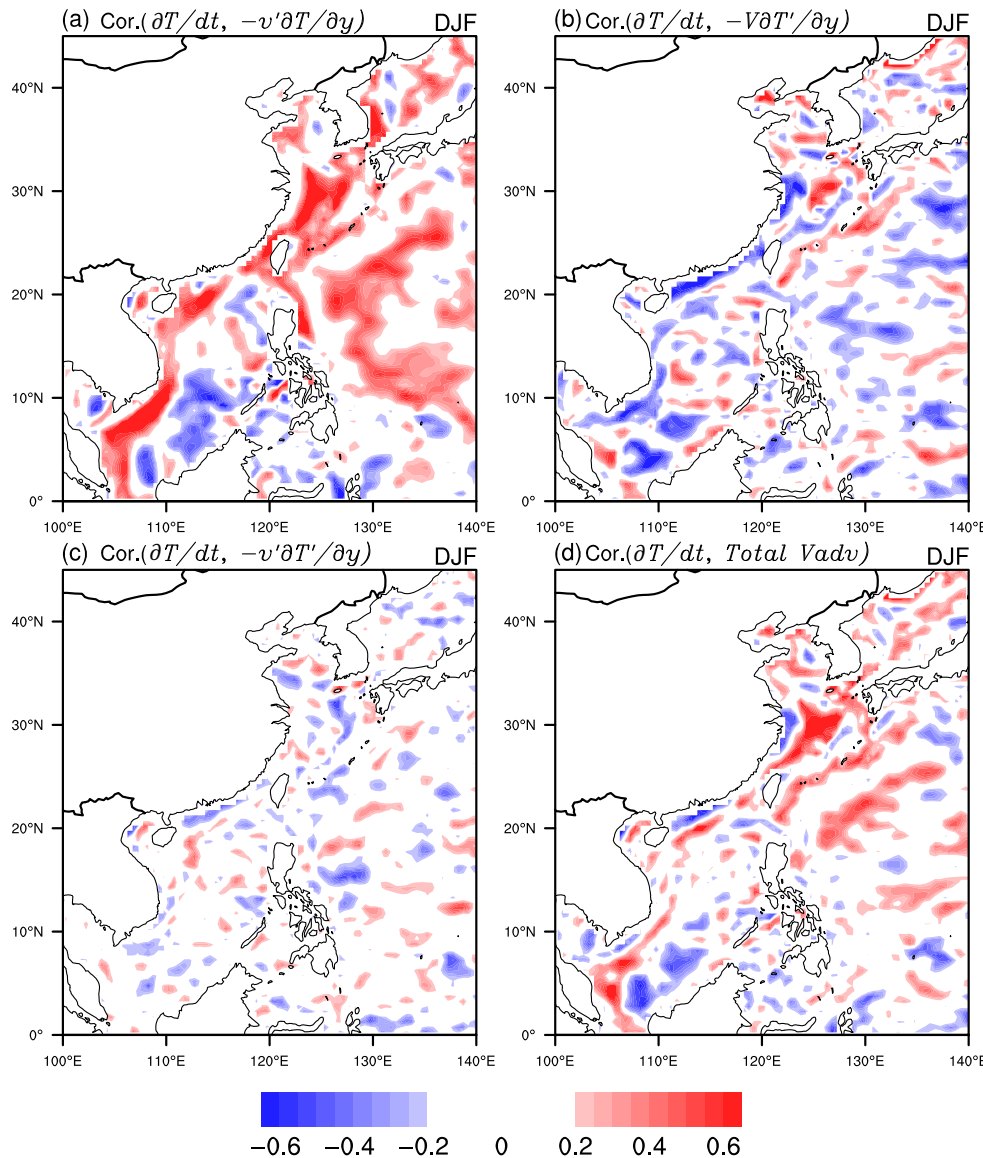


FIGURE 13 Correlation distribution of T tendency and meridional advection in winter based on CFSR (1979–2009). (a)–(d) denote correlations of $\partial T/\partial t$ to $-\bar{v}'\partial T/\partial y$, $-\bar{v}\partial T'/\partial y$, $-\bar{v}'\partial T'/\partial y$, and their sum. See text for the detailed explanation

KC. However, it should be noted that the sum contributions of Q_{net} and oceanic advection are far from the actual magnitude of T , implying that other factors also played important roles. The aim here is not to seek a complete SST budget but rather to understand the relative importance of Q_{net} and oceanic advection, as reported in previous studies (e.g., Zhang *et al.*, 2010). Around the early 2000s, the ECS experienced a pronounced cooling trend. The decrease of the ECS T (-0.4°C) occurred mainly because of the combined effects of Q_{net} (-0.2°C) and oceanic advection (-0.1°C).

Given the decadal variation of low-level wind field over the ECS, the wind-driven upper current may also contribute to the ECS warming via Ekman transport. The southern part of the ECS (south of 30°N) is dominated by the northeasterly monsoon in winter (Figure 1), which forces onshore Ekman transport of warm Kuroshio water

northeast of Taiwan (Oey *et al.*, 2013). While over the northern ECS, the prevailing northwesterly wind impedes the northward transport of warm water in terms of Ekman theory. Consequently, the warm water gathers at the southern shelf of the ECS, leading to enhanced warming in this area (Figure 6a). For a quantitative evaluation, the Ekman advection is represented by $-\vec{v}_e \cdot \nabla T$, where \vec{v}_e is the Ekman velocity and is related to the surface wind stress vector $\vec{\tau}$ by $\vec{v}_e = (\vec{\tau} \times \vec{\kappa}) / (f h)$ (Qiu, 2000; Liu *et al.*, 2014). The surface wind stress data is derived from SODA for 1979–2008, while the temperature gradient ∇T is the same as estimated in Equation (2). The magnitude of the estimated Ekman advection (Figure 15) is roughly consistent with the previous study (Liu *et al.*, 2014). There is in general an upward trend in the series of the Ekman advection from 1979 to 2008, indicating an enhanced Ekman transport (Figure 15).

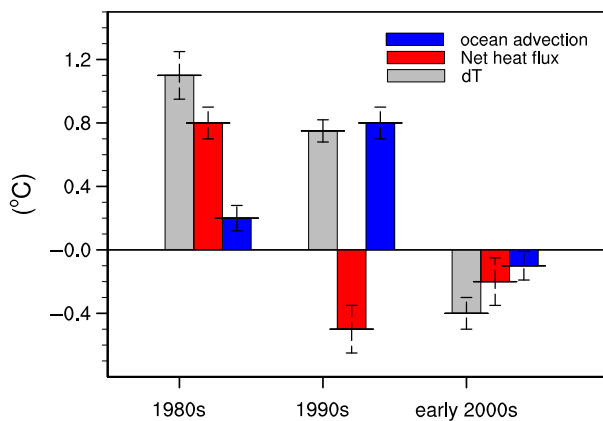


FIGURE 14 The relative contributions of net surface heat flux and total oceanic advection in change of ECS temperature anomalies, during 1980s (1980–1989), 1990s (1990–1999), and early 2000s (1999–2005). Units: $^{\circ}\text{C}$. The error bars denote standard error of the 10-year linear change

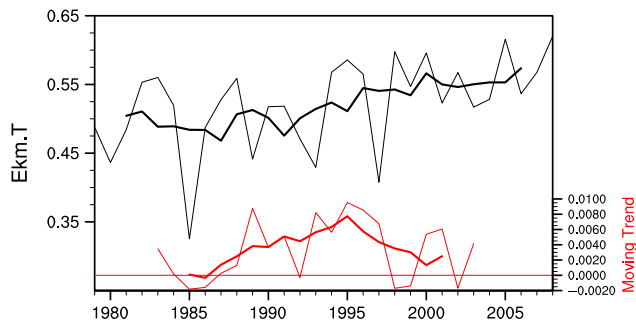


FIGURE 15 The contribution of Ekman advection ($10^{-7}\text{C}\cdot\text{s}^{-1}$, black line,) averaged from ($23\text{--}30^{\circ}\text{N}$, $121.25\text{--}122.25^{\circ}\text{E}$) for 1979–2008 and its 10-year moving trend ($10^{-7}\text{C}\cdot\text{s}^{-1}\cdot\text{year}^{-1}$, red line). The thick lines (black and red) denote 5-year running mean [Colour figure can be viewed at wileyonlinelibrary.com]

The 10-year moving trend of Ekman advection is generally consistent with that of EAWM (Figure 8). Specifically, the Ekman advection weakened during the 1980s (a negative value of 10-year moving trend in 1985), which may be in association with the contemporaneous weakening of EAWM. During the 1990s, however, the Ekman advection increased significantly, with a peak value (around $0.01 \times 10^{-7}\text{C}\cdot\text{s}^{-1}\cdot\text{year}^{-1}$) of 10-year moving trend in 1995. The estimated contribution of Ekman transport increased by about 0.3°C for the period 1990–1999. Recall that the ECS warming in 1990s is largely attributable to the oceanic advection (Figure 14), which may include the contribution of Ekman transport. During the 2000s (2000–2008), the Ekman transport also increased despite the magnitude was not so large as that in the 1990s. Hence, the increase of Ekman advection contributes

partially to the ECS warming over the past decades, especially in the 1990s.

In summary, enhanced warming or cooling in the ECS can be explained by the variations of Q_{net} and oceanic advection. In particular, Q_{net} appears the dominant contributor to the enhanced warming (cooling) in the ECS during the 1980s (early 2000s). Our results are similar to the findings of Chen et al. (2015), who suggested that surface net heat flux is predominantly responsible for the wintertime SST changes in the ECS; however, we established that oceanic advection (including the Ekman transport) played an important role in the ECS warming, especially during the 1990s.

7 | CONCLUSIONS

Based on multiple SST datasets, the present research identified an amplified response of SST in the ECS to global climate change. This amplification behaviour manifested as remarkably enhanced ECS warming rates (above 1.1 and $0.8^{\circ}\text{C}\cdot\text{decade}^{-1}$ for the 1980s and 1990s, respectively) during the global warming acceleration period, and as an obvious cooling trend (nearly $-0.5^{\circ}\text{C}\cdot\text{decade}^{-1}$) during the warming hiatus period (1998–2013). The enhanced response (warming or cooling) can be explained well by the combined effects of the KC and EAWM. The EAWM weakened dramatically around the mid-1980s, accompanied by reduced wind speeds and increased air temperatures, which impeded the release of latent and sensible heat fluxes from the ocean to the atmosphere. The reduction of surface turbulent flux resulted in rapid warming in the ECS during the 1980s. After the late 1990s, when the EAWM intensified, increased latent and sensible heat fluxes led to an enhanced cooling trend in the ECS. In addition, the volume transport of the KC to the east of Taiwan strengthened (weakened) around the mid-1990s (late 1990s), which might also in part be responsible for the enhanced warming (cooling) trend in the ECS.

As part of the North Pacific Ocean, the ECS is among the ocean regions that experienced the greatest warming during the acceleration period. However, during the hiatus period, the ECS exhibited a remarkable cooling trend, the extent of which was comparable with that of the tropical eastern Pacific Ocean, which has been identified as the major driver of the recent warming hiatus. Furthermore, the trend of the ECS SST was established as being linked closely with the phase switching of the PDO. Those periods with rapid warming (cooling) of the ECS were consistent with the maximum positive (negative) phase of the PDO. The influence of the PDO could be manifested in coastal China seas via a teleconnection that modulates

the EAWM and KC (e.g., Andres *et al.*, 2009; Kim *et al.*, 2014). In addition, the recent research reported successive record-breaking global mean temperature in association with positive phase PDO since 2014, it seems that the global warming has returned back to a new accelerated period (Su *et al.*, 2017). The ECS may experience again an enhanced warming according to the results of the present study. In short, the ECS is sensitive and potentially vulnerable to global climate change. Our research has important implications for impact assessments of climate change and for disaster preparedness in China's coastal sea regions in the face of an uncertain future climate.

ACKNOWLEDGEMENTS

We would like to thank the anonymous reviewers. This work was supported by National Key R&D Program of China (2017YFA0604901) and the Scientific Research Foundation of Third Institute, SOA (TIO2017030), the National Natural Science Foundation of China (Grant 42005013), and Opening Project of Key Laboratory of Marine Environmental Information Technology, SOA. The HadISST data was from <http://www.metoffice.gov.hk/hadobs/hadisst/>. The NCEP/ NCAR reanalysis data, ICOADS, COBE-SST, and OISST data were obtained from <http://www.ncdc.noaa.gov/>. The CFSR was from <http://rda.ucar.edu/pub/cfsr.html>. The OAFlux data were from <http://oaflux.whoi.edu>. The SODA data were retrieved from <https://climatedataguide.ucar.edu/climate-data/soda-simple-ocean-data-assimilation/>.

ORCID

Hongjian Tan  <https://orcid.org/0000-0002-9885-8819>

REFERENCES

- Andres, M., Park, J.-H., Wimbush, M., Zhu, X.-H., Nakamura, H., Kim, K. and Chang, K.-I. (2009) Manifestation of the Pacific Decadal Oscillation in the Kuroshio. *Geophysical Research Letters*, 36, L16602. <https://doi.org/10.1029/2009GL039216>.
- Belkin, I.M. (2009) Rapid warming of large marine ecosystems. *Progress in Oceanography*, 81, 207–213.
- Cai, R., Tan, H. and Kontoyiannis, H. (2017) Robust surface warming in offshore China seas and its relationship to the east Asian monsoon wind field and ocean forcing on interdecadal time scales. *Journal of Climate*, 30(22), 8987–9005.
- Cai, R., Tan, H. and Qi, Q. (2016) Impacts of and adaptation to inter-decadal marine climate change in coastal China seas. *International Journal of Climatology*, 36(11), 3770–3780. <https://doi.org/10.1002/joc.4591>.
- Carton, J. A. and Giese, B. S. (2008) A reanalysis of ocean climate using Simple Ocean Data Assimilation (SODA). *Monthly Weather Review*, 136, 2999–3017. <https://doi.org/10.1175/2007MWR1978.1>.
- Chen, W., Feng, J. and Wu, R. (2013) Roles of ENSO and PDO in the link of the East Asian winter monsoon to the following summer monsoon. *Journal of Climate*, 26, 622–635.
- Chen, Z., Wu, R. and Chen, W. (2015) Effects of northern and southern components of the East Asian winter monsoon variability on SST changes in the western North Pacific. *Journal of Geophysical Research – Atmospheres*, 120(9), 3888–3905. <https://doi.org/10.1002/2015JD023149>.
- Dai, A., Fyfe, J.C., Xie, S.-P. and Dai, X. (2015) Decadal modulation of global surface temperature by internal climate variability. *Nature Climate Change*, 5(6), 555–559. <https://doi.org/10.1038/nclimate2605>.
- Duchon, C.E. (1979) Lanczos filtering in one and two dimensions. *Journal of Applied Meteorology*, 18(8), 1016–1022.
- England, M.H., McGregor, S., Spence, P., Meehl, G.A., Timmermann, A., Cai, W., Gupta, A.S., McPhaden, M.J., Purich, A. and Santoso, A. (2014) Recent intensification of wind-driven circulation in the Pacific and the ongoing warming hiatus. *Nature Climate Change*, 4(3), 222–227.
- Guo, X., Miyazawa, Y. and Yamagata, T. (2006) The Kuroshio onshore intrusion along the shelf break of the East China Sea: the origin of the Tsushima Warm Current. *Journal of Physical Oceanography*, 36(12), 2205–2231.
- Hsin, Y.-C., Wu, C.-R. and Shaw, P.-T. (2008) Spatial and temporal variations of the Kuroshio east of Taiwan, 1982–2005: a numerical study. *Journal of Geophysical Research*, 113, C04002. <https://doi.org/10.1029/2007JC004485>.
- Huang, J., Zhang, X., Zhang, Q., Lin, Y., Hao, M., Luo, Y., Zhao, Z., Yao, Y., Chen, X. and Wang, L. (2017) Recently amplified arctic warming has contributed to a continual global warming trend.. *Nature Climate Change*, 7(12), 875–879.
- IPCC. (2013) *Climate change 2013: the physical science basis*. In: Stocker, T.F., Qin, D., Plattner, G. K., Tignor, M., Allen, S. K., Boschung, J., Nauels, A., Xia, Y., Bex, V. & Midgley, P. M., (Eds.) Contribution of Working Group I to the Fifth Assessment Report of the Intergovernmental Panel on Climate Change, pp. 1535–2. Cambridge, UK and New York, NY: Cambridge University Press. <https://doi.org/10.1017/CBO9781107415324>.
- Jia, F., Wu, L., Gan, B. and Cai, W. (2016) Global warming attenuates the tropical Atlantic-Pacific teleconnection. *Scientific Reports*, 6(1), 20078.
- Kako, S., Nakagawa, T., Takayama, K., Hirose, N. and Isobe, A. (2016) Impact of Changjiang River discharge on sea surface temperature in the East China Sea. *Journal of Physical Oceanography*, 46(6), 1735–1750.
- Kalnay, E., Kanamitsu, M., Kistler, R., Collins, W., Deaven, D., Gandin, L., Iredell, M., Saha, S., White, G., Woollen, J. and Zhu, Y. (1996) The NCEP/NCAR 40-year reanalysis project. *Bull. Am. Meteorol. Soc.*, 77(3), 437–471.
- Karl, T.R., Arguez, A., Huang, B., Lawrimore, J.H., McMahon, J.R., Menne, M.J., Peterson, T.C., Vose, R.S. and Zhang, H.M. (2015) Possible artifacts of data biases in the recent global surface warming hiatus. *Science*, 348(6242), 1469–1472.
- Kelly, K.A. and Qiu, B. (1995) Heat flux estimates for the western North Atlantic. Part II: the upper-ocean heat balance. *Journal of Physical Oceanography*, 25(10), 2361–2373.
- Kim, J.W., Yeh, S.W. and Chang, E.C. (2014) Combined effect of El Niño-southern oscillation and Pacific decadal oscillation on the east Asian winter monsoon. *Climate Dynamics*, 42(3–4), 957–971.
- Kosaka, Y. and Xie, S.-P. (2013) Recent global-warming hiatus tied to equatorial Pacific surface cooling. *Nature*, 501(7467), 403–407.

- Liao, E., Lu, W., Yan, X.-H., Jiang, Y. and Kidwell, A. (2015) The coastal ocean response to the global warming acceleration and hiatus. *Scientific Reports*, 5, 16630. <https://doi.org/10.1038/srep16630>.
- Liu, Q.-Y., Wang, D., Wang, X., Shu, Y., Xie, Q. and Chen, J. (2014) Thermal variations in the South China Sea associated with the eastern and Central Pacific El Niño events and their mechanisms. *Journal of Geophysical Research: Oceans*, 119, 8955–8972. <https://doi.org/10.1002/2014JC010429>.
- Medhaug, I., Stolpe, M.B., Fischer, E.M. and Knutti, R. (2017) Reconciling controversies about the 'global warming hiatus'. *Nature*, 545(7652), 41–47.
- Moisan, J.R. and Niiler, P.P. (1998) The seasonal heat budget of the North Pacific: net heat flux and heat storage rates (1950–1990). *Journal of Physical Oceanography*, 28, 401–421.
- Morice, C.P., Kennedy, J.J., Rayner, N.A. and Jones, P.D. (2012) Quantifying uncertainties in global and regional temperature change using an ensemble of observational estimates: the HadCRUT4 data set. *Journal of Geophysical Research*, 117, D08101. <https://doi.org/10.1029/2011JD017187>.
- Oey, L.Y., Chang, M.C., Chang, Y.L., Lin, Y.C. and Xu, F.H. (2013) Decadal warming of coastal China Seas and coupling with winter monsoon and currents. *Geophysical Research Letters*, 40, 6288–6292. <https://doi.org/10.1002/2013GL058202>.
- Met Offie. (2013) *The Recent Pause in Global Warming (1): What Do Observations of the Climate System Tell us?*. Exeter, Devon: Met Offie, pp. 1–2.
- Qiu, B. (2000) Interannual variability of the Kuroshio extension system and its impact on the wintertime SST field. *Journal of Physical Oceanography*, 30, 1486–1502.
- Rayner, N.A., et al. (2003) Global analyses of sea surface temperature, sea ice, and night marine air temperature since the late nineteenth century. *Journal of Geophysical Research: Atmospheres*, (1984–2012), 108(D14), 4407. <https://doi.org/10.1029/2002JD002670>.
- Saha, S., Moorthi, S., Pan, H.L., Wu, X., Wang, J., Nadiga, S., Tripp, P., Kistler, R., Woollen, J., Behringer, D., Liu, H., Stokes, D., Grumbine, R., Gayno, G., Wang, J., Hou, Y.T., Chuang, H.Y., Juang, H.M.H., Sela, J., Iredell, M., Treadon, R., Kleist, D., van Delst, P., Keyser, D., Derber, J., Ek, M., Meng, J., Wei, H., Yang, R., Lord, S., van den Dool, H., Kumar, A., Wang, W., Long, C., Chelliah, M., Xue, Y., Huang, B., Schemm, J.K., Ebisuzaki, W., Lin, R., Xie, P., Chen, M., Zhou, S., Higgins, W., Zou, C.Z., Liu, Q., Chen, Y., Han, Y., Cucurull, L., Reynolds, R.W., Rutledge, G. and Goldberg, M. (2010) The NCEP climate forecast system reanalysis. *Bulletin of the American Meteorological Society*, 91, 1015–1057.
- Steinman, B.A., Mann, M.E. and Miller, S.K. (2015) Atlantic and Pacific multidecadal oscillations and Northern Hemisphere temperatures. *Science*, 347(6225), 988–991.
- Su, J., Zhang, R. and Wang, H. (2017) Consecutive record-breaking high temperatures marked the handover from hiatus to accelerated warming. *Scientific Reports*, 7, 43735. <https://doi.org/10.1038/srep43735>.
- Tanimoto, Y., Nakamura, H., Kagimoto, T. and Yamane, S. (2003) An active role of extratropical sea surface temperature anomalies in determining anomalous turbulent heat flux. *Journal of Geophysical Research*, 108(C10), 3304. <https://doi.org/10.1029/2002JC001750>.
- Trenberth, K.E. (1984) Signal versus noise in the southern oscillation. *Monthly Weather Review*, 112(2), 326–332.
- Trenberth, K.E., Fasullo, J.T., Branstator, G. and Phillips, A.S. (2014) Seasonal aspects of the recent pause in surface warming. *Nature Climate Change*, 4(10), 911–916. <https://doi.org/10.1038/nclimate2341>.
- Wang, B. (1992) The vertical structure and development of the ENSO anomaly mode during 1979–1989. *Journal of the Atmospheric Sciences*, 49, 698–712.
- Wang, L. and Chen, W. (2014a) The East Asian winter monsoon: re-amplification in the mid-2000s. *Chinese Science Bulletin*, 59 (4), 430–436.
- Wang, L. and Chen, W. (2014b) An intensity index for the East Asian winter monsoon. *Journal of Climate*, 27(6), 2361–2374.
- Wang, L., Chen, W. and Huang, R. (2008) Interdecadal modulation of PDO on the impact of ENSO on the East Asian winter monsoon. *Geophysical Research Letters*, 35(20), L20702. <https://doi.org/10.1029/2008GL035287>.
- Wang, L. and Lu, M.-M. (2017) The East Asian winter monsoon. In: Chang, C.-P., et al. (Eds.) *The Global Monsoon System: Research and Forecast*, 3rd edition, pp. 51–61. Singapore: World Scientific. https://doi.org/10.1142/9789813200913_0005.
- Watanabe, M., et al. (2014) Contribution of natural decadal variability to global warming acceleration and hiatus. *Nature Climate Change*, 4(10), 893–897. <https://doi.org/10.1038/NCLIMATE2355>.
- Wu, L., Cai, W., Zhang, L., Nakamura, H., Timmermann, A., Joyce, T., McPhaden, M.J., Alexander, M., Qiu, B., Visbeck, M., Chang, P. and Giese, B. (2012) Enhanced warming over the global subtropical western boundary currents. *Nature Climate Change*, 2(3), 161–166.
- Wu, R., Chen, W., Huang, G. and Hu, K. (2014) Relative contribution of ENSO and East Asian winter monsoon to the South China Sea SST anomalies during ENSO decaying years. *Journal of Geophysical Research – Atmospheres*, 119(9), 5046–5064.
- Yeh, S.W. and Kim, C.H. (2010) Recent warming in the yellow/East China Sea during winter and the associated atmospheric circulation. *Continental Shelf Research*, 30(13), 1428–1434.
- Zhang, L., Wu, L., Lin, X., et al. (2010) Modes and mechanisms of sea surface temperature low-frequency variations over the coastal China seas. *Journal of Geophysical Research: Oceans*, 115(C8), C08031. <https://doi.org/10.1029/2009JC006025>.
- Zhou, Z.Q., Xie, S.P., Zheng, X.T., Liu, Q. and Wang, H. (2014) Global warming-induced changes in El Niño teleconnections over the north Pacific and North America. *Journal of Climate*, 27(24), 9050–9064.

SUPPORTING INFORMATION

Additional supporting information may be found online in the Supporting Information section at the end of this article.

How to cite this article: Tan H, Cai R, Yan X, Li C. Amplification of Winter Sea surface temperature response over East China Seas to global warming acceleration and slowdown. *Int J Climatol*. 2021;41:2082–2099. <https://doi.org/10.1002/joc.6948>